PNAS RESEARCH ARTICLE | MICROBIOLOGY

Genome-wide and targeted CRISPR screens identify RNF213 as a mediator of interferon gamma–dependent pathogen restriction in human cells

Sumit K. Matta[a], Hinissan P. Kohio[a,1], Pallavi Chandra[b,1], Adam Brown[c], John G. Doench[c], Jennifer A. Philips[a,b], Siyuan Ding[a], and L. David Sibley[a,2]

Contributed by L. David Sibley; received September 14, 2023; accepted November 15, 2023; reviewed by Peter Murray, Klaus Pfeffer, and Masahiro Yamamoto

To define cellular immunity to the intracellular pathogen *Toxoplasma gondii*, we performed a genome-wide CRISPR loss-of-function screen to identify genes important for (interferon gamma) IFN-γ-dependent growth restriction. We revealed a role for the tumor suppressor *NF2/Merlin* for maximum induction of Interferon Stimulated Genes (ISG), which are positively regulated by the transcription factor IRF-1. We then performed an ISG-targeted CRISPR screen that identified the host E3 ubiquitin ligase *RNF213* as necessary for IFN-γ-mediated control of *T. gondii* in multiple human cell types. *RNF213* was also important for control of bacterial (*Mycobacterium tuberculosis*) and viral (Vesicular Stomatitis Virus) pathogens in human cells. RNF213-mediated ubiquitination of the parasitophorous vacuole membrane (PVM) led to growth restriction of *T. gondii* in response to IFN-γ. Moreover, overexpression of RNF213 in naive cells also impaired growth of *T. gondii*. Surprisingly, growth inhibition did not require the autophagy protein ATG5, indicating that RNF213 initiates restriction independent of a previously described noncanonical autophagy pathway. Mutational analysis revealed that the ATPase domain of RNF213 was required for its recruitment to the PVM, while loss of a critical histidine in the RZ finger domain resulted in partial reduction of recruitment to the PVM and complete loss of ubiquitination. Both RNF213 mutants lost the ability to restrict growth of *T. gondii*, indicating that both recruitment and ubiquitination are required. Collectively, our findings establish RNF213 as a critical component of cell-autonomous immunity that is both necessary and sufficient for control of intracellular pathogens in human cells.

interferon | anti-viral | STAT1 signaling | CRISPR/Cas9 | genome-wide screen

Significance

Interferons provide protection against pathogens by inducing the expression of genes encoding defense proteins that often directly target invading pathogens. Previous studies have identified several such effectors that can defend against intracellular parasites; however, their roles tend to be partial and limited to specific cell types. Here, we used genome-wide and targeted CRISPR screens to search in an unbiased way for a general regulator of pathogen restriction in response to interferon gamma. We identified an E3 ligase called RNF213 that decorates the pathogen containing vacuole with ubiquitin, thus imparting growth restriction. RNF213 acts against viruses, bacteria, and protozoan parasites and provides a major mechanism for resistance against intracellular parasites in a variety of human cell types.

Toxoplasma gondii is a widespread parasite of animals that also frequently causes zoonotic infection in humans. As an obligate intracellular parasite, *T. gondii* resides within a specialized vacuole that is largely sequestered from the host endomembrane system, which provides a niche for intracellular growth (1). Cell-autonomous mechanisms for immune control of intracellular *T. gondii* are best known form studies in laboratory mice (2, 3). Type II interferon, or interferon gamma (IFN-γ), plays the major role in resistance to infection in the mouse (4, 5), while type I interferon also contributes to control of infection (6), particularly in the central nervous system during chronic infection (7). Treatment with IFNs leads to upregulation of numerous Interferon Stimulated Genes (ISGs), the exact complement of which varies by cell type (8, 9). Among the most strongly up-regulated ISGs are the critically important immunity-related GTPases (IRGs) and guanylate-binding proteins (GBPs), which collectively lead to vacuole rupture, parasite destruction, and clearance in murine cells (10–12). The IRG/GBP system is under control of a noncanonical autophagy (ATG) system that requires core ATG components for conjugation of LC3 to phosphatidyl ethanolamine (PE), but it does not require the initiation nor degradative steps (13–15). Although, IRGs and GBPs play a central role in immunity in rodents, human cells largely lack IRGs and GBPs have been described to play a more limited role, as discussed further below.

Clinical evidence that human cells control intracellular *T. gondii* via an interferon-mediated process comes from studies demonstrating that immunocompromised patients with low levels of IFN-γ are susceptible to reactivation of latent toxoplasmosis (16). In vitro studies indicate that multiple IFN-γ-dependent pathways can mediate growth restriction in humans. Although humans are not natural hosts in the life cycle, human macrophages are nonetheless able to control the replication of intracellular *T. gondii* in response to IFN-γ (17, 18) and IFN-β (19, 20). Nonhematopoietic human cells also control intracellular *T. gondii* through varied and often cell type–specific mechanisms (21). For example, induction of indole-2,3-dioxygenase (IDO1) by interferon leads to degradation of tryptophan, thus

Reviewers: P.M., Max Planck Institute for Biochemistry; K.P., Institute of Medical Microbiology and Hospital Hygiene, Heinrich-Heine-University Duesseldorf; and M.Y., Research Institute for Microbial Diseases, Osaka Daigaku.

The authors declare no competing interest.

[1]H.P.K. and P.C. contributed equally to this work.

[2]To whom correspondence may be addressed. Email: sibley@wustl.edu.

This article contains supporting information online at https://www.pnas.org/lookup/suppl/doi:10.1073/pnas.2315865120/-/DCSupplemental.

Published December 26, 2023.

limiting parasite growth in human fibroblasts (22) and human brain microvascular endothelial cells (23). In addition, the noncanonical autophagy pathway described above is required for recruitment of LC3, leading to engulfment of the parasite containing vacuole in multiple membranes, a process that is associated with growth restriction in Hela cells (24), A549 cells (25), and human umbilical vein endothelial cells (26). Curiously, the ATG-dependent growth restriction is not global (14) but rather limited to those vacuoles that become ubiquitinated and acquire adaptors such as p62, NDP52, and LC3 (24, 26). Virulent type I strains are largely resistant to this pathway, while types II and III are susceptible (24), although the basis for this difference is unknown. Recent studies identified the E3 ubiquitin ligase RNF213 in early ubiquitination and subsequent recruitment of autophagy adaptor proteins (e.g., p62, NDP52, optineurin) to *T. gondii* –containing vacuoles in IFN-γ-treated A549 cells (27). The IFN-γ signaling and noncanonical ATG pathways are connected by ISG15, which is required for maximal recruitment of ATG adaptors and also interacts with RNF213 (25). Additionally, GBP1 has been implicated in restricting *T. gondii* growth in human epithelial cells, despite not being recruited to the vacuole (28), although it is recruited to the vacuole membrane in THP-1 cells, resulting in rupture and activation of apoptosis (29). GBP2 and GBP5 also contribute to growth restriction in THP-1 cells, despite not being recruited to the parasite containing vacuole (30). Collectively, these prior candidate-gene studies indicate that multiple IFN-γ-dependent mechanisms can contribute to growth restriction, which is often partial and expressed in a cell-specific manner. However, the absence of any prior global or unbiased assessment of genes required for IFN-γ-mediated growth restriction leaves open the possibility that an additional IFN-γ-mediated pathway exists in all or most human cells. To provide an unbiased assessment of the predominate pathways for control of *T. gondii* growth in IFN-γ-activated human cells, we performed genome-wide and targeted ISG CRISPR screens in A549 cells.

Results

Genome-Wide CRISPR Screen Identifies Factors Important for IFN-γ-Mediated Growth Restriction. To facilitate CRISPR screening, we developed a growth restriction assay using a previously described vacuole size assay (7) to monitor growth of the susceptible *T. gondii* type III strain CTG (24) in IFN-γ-treated A549 cells. Quantification of vacuole size after IFN-γ treatment verified that wild-type (WT) cells restricted parasite expansion and that this ability was abrogated in *STAT1* knockout (STAT1-KO) cells (Fig. 1*A* and *SI Appendix*, Fig. S1*A*). As expected, the growth restriction was independent of exogenously added tryptophan, indicating that it does not rely on IDO1, as previously reported (31). To develop a process for selecting cells from the population, we infected A549 cells with a recombinant CTG strain expressing green fluorescent protein (GFP) (CTG-GFP), trypsinized cells from the dish, and analyzed them by flow cytometry to evaluate the average intensity of GFP as a proxy for parasite growth (Fig. 1*B*). Although there was not a distinct separation between the populations of CTG-GFP in WT vs. STAT1-KO cells, there was a clear shoulder of higher GFP expression in the STAT1-KO cells (green box, Fig. 1*B*). We therefore reasoned that escape mutants that lose the ability to control parasite replication should mimic the growth of CTG-GFP in STAT1-KO cells, thus providing the basis for the CRISPR-based screens described below.

We transduced A549 cells with the Brunello library containing four guides each to ~20,000 genes in the human genome (32) and developed a screen for loss of IFN-γ-mediated growth restriction (Fig. 1*C*). To perform the screen, A549 cells were activated with IFN-γ, infected with CTG-GFP, and the top 5% of GFP expressing cells were sorted from four independent experiments (Fig. 1*D*). The sgRNAs from these pools were amplified, barcoded, and subjected to NGS sequencing. Comparison of the guide abundances in the top 5% relative to a time-matched point for the uninfected pool was used to classify guides that were significantly different based on fold change and FDR (false discovery rate) in the four replicates of the primary screen (Fig. 1*E* and Dataset S1). There was a high degree of variability in genes that scored significant between the various replicates. For example, only five genes (including *NF2* and *FRYL*) were significant in all four replicates when analyzed separately (*SI Appendix*, Fig. S1*B*). Additionally, 23 genes were individually significant in 3 of 4 while 224 were significant in 2 of 4 replicates (*SI Appendix*, Fig. S1*B*). However, using the more stringent criteria of FDR for the combined replicates, only *NF2* and *FRYL* were significant (Fig. 1*E*). Although guides for *STAT1* and *IRF1* were slightly enriched, the strongest signal for enhanced sgRNA guides corresponded to the gene *NF2* (Neurofibromatosis 2), an Ezrin/Radixin/Moesin family member that is also known as *MERLIN*, and which functions as a tumor suppressor (Fig. 1*E*) (33). We also detected three genes that showed reduced sgRNAs (*PTEN*, *TSC1*, and *TSC2*) (Fig. 1*E*), which presumably are depleted because cells lacking these genes have decreased survival during infection and IFN-γ treatment.

Secondary Pool CRISPR Screen Identifies IFN-γ-STAT1 Axis and NF2 as Critical for Growth Restriction. Comparison of the results from the primary screen revealed a high degree of variability in genes classified as significantly different between the replicates, similar to prior FACS-based screens (34). To account for the possibility that the genome-wide screen missed genes that contribute to IFN-γ-mediated resistance, we developed a secondary screen based on a pool of genes that were significantly enriched in at least 2 of 4 replicates of the primary screen (*SI Appendix*, Fig. S1*B*). The secondary screen included 224 genes with coverage of 10 sgRNAs per gene, thus improving statistical power for identifying differences. The secondary screen identified several factors in the IFN-γ-STAT1 axis and their loss indicates that they are essential for growth restriction (Fig. 1*F*) (Dataset S2). Included in the set of highly enriched guides, which represent depleted genes, were *STAT1*, the *JAK2* kinase that phosphorylates STAT1, the IFN-γ receptor subunits *IFNGR1* and *IFNGR2* as well as the downstream transcription factor *IRF-1*, which augments the activity of IFN-γ on inducing gene expression (35) (Fig. 1*F*). The only gene not part of the IFN-γ-STAT1 pathway was *NF2*, which was the top hit in the primary screen (Fig. 1*F*). The four other genes that were significantly enriched in each replicate of primary screen, including *FRYL*, were not enriched in the top 5% population of the secondary screen.

To elucidate the contribution of NF2 to cell-autonomous pathogen control, we generated KOs using lentiviral transduction and targeted CRISPR-Cas9 gene editing for both *IRF-1* and *NF2* in A549 cells (*SI Appendix*, Fig. S2 *A* and *B*). As expected, IRF-1 showed dependence for expression in WT cells and NF2-KO cells on IFN-γ treatment, while NF2 was not affected by IFN-γ treatment (Fig. 2*A*). NF2 was not localized to the parasitecontaining vacuole and instead was localized on the host plasma membrane in A549 cells (*SI Appendix*, Fig. S2*C*). We then ascertained the ability of IFN-γ to control growth of CTG parasites in WT, IRF-1 KO, or NF2 KO cells using the vacuole size assay. As expected, growth restriction seen in WT cells was completely lost in IRF-1 KO cells, consistent with previous reports that this transcription factor is essential for control of *T. gondii* in IFN-γ-treated cells (31). In contrast, loss of NF2 resulted in a partial, yet significant reduction in the growth restriction following IFN-γ (Fig. 2 *B* and *C*).

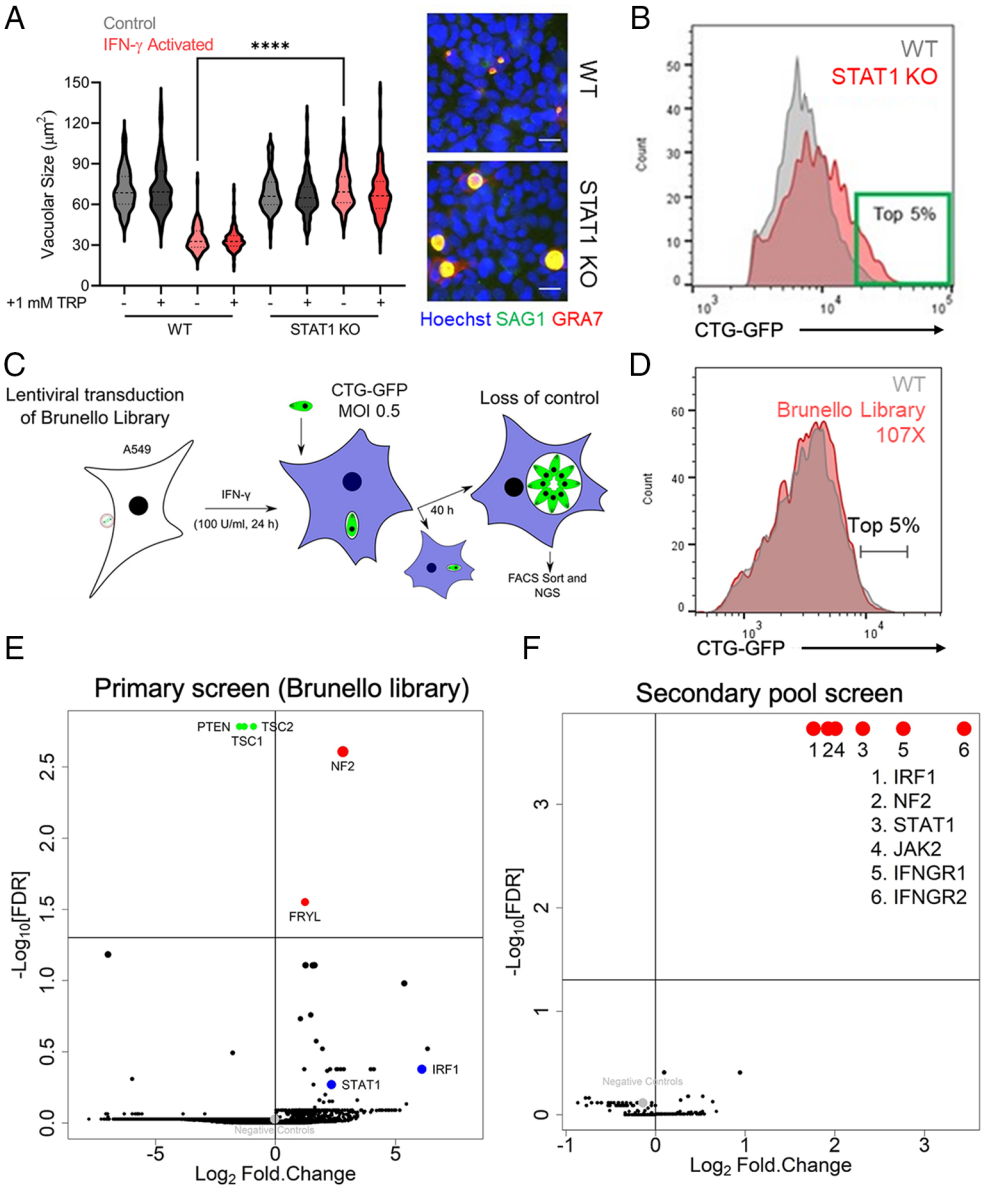

Fig. 1. Design and implementation of genome-wide CRISPR screens for loss of IFN-γ-mediated parasite growth restriction in human cells. (*A*) Tryptophan (TRP)-independent restriction of *T. gondii* in lung alveolar epithelial A549 cells. WT and STAT1 knock out (KO) A549 cells (*SI Appendix*, Fig. S1*A*) were treated ± IFN-γ (100 Units/mL) 24 h prior to infection with type III CTG strain of *T. gondii.* Samples consist of untreated control (circles) or supplemented with 1 mM TRP (triangles). Growth was measured by vacuolar size (μ^2) in three biological replicates with at least 30 images per sample. The violin plot shows mean vacuolar size per. Statistical analysis: ****$P < 0.0001$ using an unpaired two-tailed Student's *t* test with Welch's correction. Examples show representative images of WT and STAT1 KO A549 cells (+IFN-γ +TRP) infected with CTG and analyzed at 40 h hpi. Nuclei were labeled with Hoechst (blue), parasites with anti-SAG1 (green), and the vacuole was labeled with anti-GRA7 (red). (Scale bar, 20 μ.) (*B*) IFN-γ-activated WT vs. STAT1 KO A549 cells infected with CTG expressing GFP (CTG-GFP) were fixed 40 hpi and analyzed by flow cytometry. The histogram shows GFP-positive (CTG-GFP infected) cells. The green box defines the top 5% of CTG-GFP expressing cells. (*C*) Design of genome-wide CRISPR-Cas9 to identify factors involved in IFN-γ-mediated parasite growth restriction in human (A549) cells. (*D*) The Brunello library (32) was transduced into A549 cells at ~100X coverage. Graph depicts results of CTG-GFP infection analyzed at 40 hpi in IFN-γ-activated control (WT) and Brunello library transduced A549 cells. (*E*) Primary genome-wide CRISPR screen showing $\log_2$ fold change in sgRNAs from the top 5% of CTG-GFP expressing cells (T5) compared to uninfected cells plotted against $-\log_{10}$ FDR for all four independent replicates combined. Genes for significantly enriched sgRNAs (red) vs. significantly depleted sgRNAs in the T5 pool (green) are labeled. *STAT1* and *IRF1* (blue dots) are marked to identify positive controls for the experiment. (*F*) Secondary CRISPR screen consisting of a subpool of 224 genes that were significantly enriched in the T5 population ($\log_2$ fold change > 1 and $P < 0.05$) in at least 2 out of the 4 replicates of the primary Brunello screen (*SI Appendix*, Fig. S1*B*). $\log_2$ fold change is plotted against $-\log_{10}$ FDR for all four independent replicates combined.

Loss of NF2 Down-Modulates IRF-1-Dependent ISG Expression. To further explore the role of NF2 in IFN-γ-dependent growth restriction, we compared the transcriptional profile of WT, IRF-1 KO, or NF2 KO cells under resting and activated conditions. Comparison of the NF2 KO to WT cells revealed multiple of genes that were NF2 dependent (*SI Appendix*, Fig. S2*C*), which likely reflect its diverse roles. However, when we compared the IFN-γ induced genes that were IRF-1-dependent, there was a clear pattern that most of these genes were also dampened in the NF2 KO (*SI Appendix*, Fig. S2*E*). Loss of NF2 in A549 cells led to an average reduction of ~25% Log2 expression in IFN-γ-mediated induction of IRF-1-dependent genes (Fig. 2*D*). The influence of NF2 on expression of IRF-1-dependent genes varied between different subclusters and was generally higher for genes present in subclusters 1 and 4 (Fig. 2*E* and *SI Appendix*, Fig. S2*E*). For example, *IDO1* (subcluster 1) and *RARESS3* (subcluster 4) were more strongly affected by loss of *NF2* (Fig. 2*F*), whereas *APOL3* (subcluster 2) and *OAS3* (subcluster 5) were only partially affected by loss of NF2 (Fig. 2*F*). We also examined the effect of NF2 on IFN-β driven expression using an ISRE (Interferon Stimulation

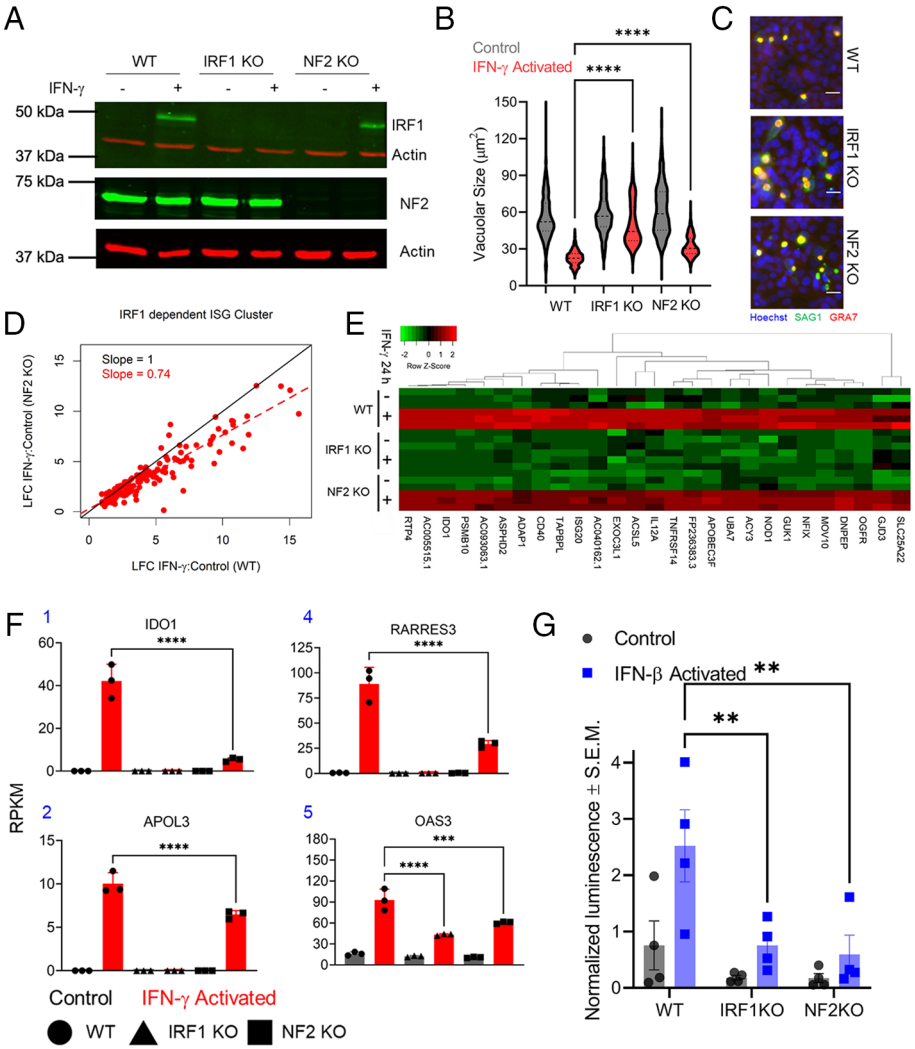

Fig. 2. NF2 dampens IFN-γ-mediated growth restriction by inhibiting ISG induction. (*A*) Immunoblots for IRF1 and NF2 in WT, IRF1 KO, and NF2 KO A549 cells (*SI Appendix*, Fig. S2 *A* and *B*). Actin was used as a loading control. (*B*) WT, IRF1 KO, and NF2 KO A549 cells treated ± IFN-γ (100 U/mL) for 24 h, infected with CTG strain *parasites*, and evaluated for growth restriction at 40 hpi. Violin plots show mean vacuolar size per image three biological replicates containing at least 30 images per sample. Statistical analysis: ****$P < 0.0001$ using the Kruskal–Wallis test with Dunn's multiple comparison test. (*C*) Representative images of IFN-γ-activated WT, IRF1 KO, and NF2 KO A549 cells infected with CTG and analyzed at 40 hpi. Staining: nuclei Hoechst (blue), parasites anti-SAG1 (green), and vacuoles anti-GRA7 (red). (Scale bar, 20 μ.) (*D*) Log_2 fold change plot of genes (IRF1 dependent) induced upon IFN-γ stimulation compared to untreated control in WT (*x*-axis) and NF2 KO (*y*-axis) A549 cells. The red line shows linear regression. (*E*) The heatmap depicts genes from subcluster 1 (*SI Appendix*, Fig. S2*E*) that were induced in WT but not in IRF1 KO cells from three biological replicates (log_2 fold change > 1 and $P < 0.05$) clustered using 1-Pearson distance and complete linkage on normalized log_2 (RPKM). Normalized Z-scores are color-scaled from downregulation (green) to upregulation (red). (*F*) RPKM values showing partial induction of select ISGs in NF2 KO cells compared to WT cells upon IFN-γ activation. Examples chosen from IRF1-dependent gene subclusters 1 (*IDO1*), 2 (*APOL3*), 4 (*RARRES3*), and 5 (*OAS3*). Statistical analyses: ***$P < 0.001$ and ****$P < 0.0001$ using one-way ANOVA with Šídák's multiple comparisons test. (*G*) ISRE promoter activity from A549 cells transfected with ISRE reporter plasmid expressing Gaussia luciferase (7) and control pCMV-Red Firefly Luc plasmid (Thermo Fisher Scientific) for 24 h. The bar plot shows mean ± SEM. Gaussia luciferase activity normalized to firefly luciferase activity for four independent biological replicates. Statistical analysis: *$P < 0.05$ using two-way ANOVA with Tukey's multiple comparison test.

Response Element) promoter normalized to constitutively expressed firefly luciferase. Induction of ISRE activity by IFN-β was significantly diminished in both IRF1 KO and NF2 KO cells (Fig. 2*G*), indicating that both factors likely also participate in IRF-1-mediated transcription. In summary, although NF2 has not previously been identified as part of the IFN-γ response pathway, it is necessary for maximum induction of ISGs in response to both type I and type II IFN.

ISG-Targeted CRISPR Screen Identifies RNF213 as the Primary Determinant of IFN-γ-Mediated Growth Restriction in Multiple Human Cell Types. We were surprised that neither the primary nor secondary genome-wide screens identified any canonical ISGs, except for the broadly acting transcription factor IRF-1. Consequently, we designed a focused CRISPR screen based on a previous set of ISGs that was defined by transcriptional induction in response to IFN-γ in A549 cells (31). The ISG screen included ~350 genes with coverage at 10 sgRNAs per gene and was repeated four times independently (Fig. 3*A*). Sequencing the top 5% of CTG-GFP-positive cells was used to define sgRNAs that were significantly enriched, thus identifying genes important for IFN-γ-mediated control. We identified only a single strong positive corresponding the gene E3 ligase *RNF213*, in addition to *IRF-1* (Fig. 3*B*) (Dataset S3). RNF213 was constitutively expressed at moderate levels in A549 cells and yet was also up-regulated by treatment with IFN-γ or IFN-β in a dose-dependent manner (*SI Appendix*, Fig. S3 *A* and *B*). Considering the prominent signal detected in the ISG CRISPR screen, we wondered why *RNF213*was not detected in the primary or secondary genome-wide CRISPR screens. *RNF213* ranked 304 in the primary

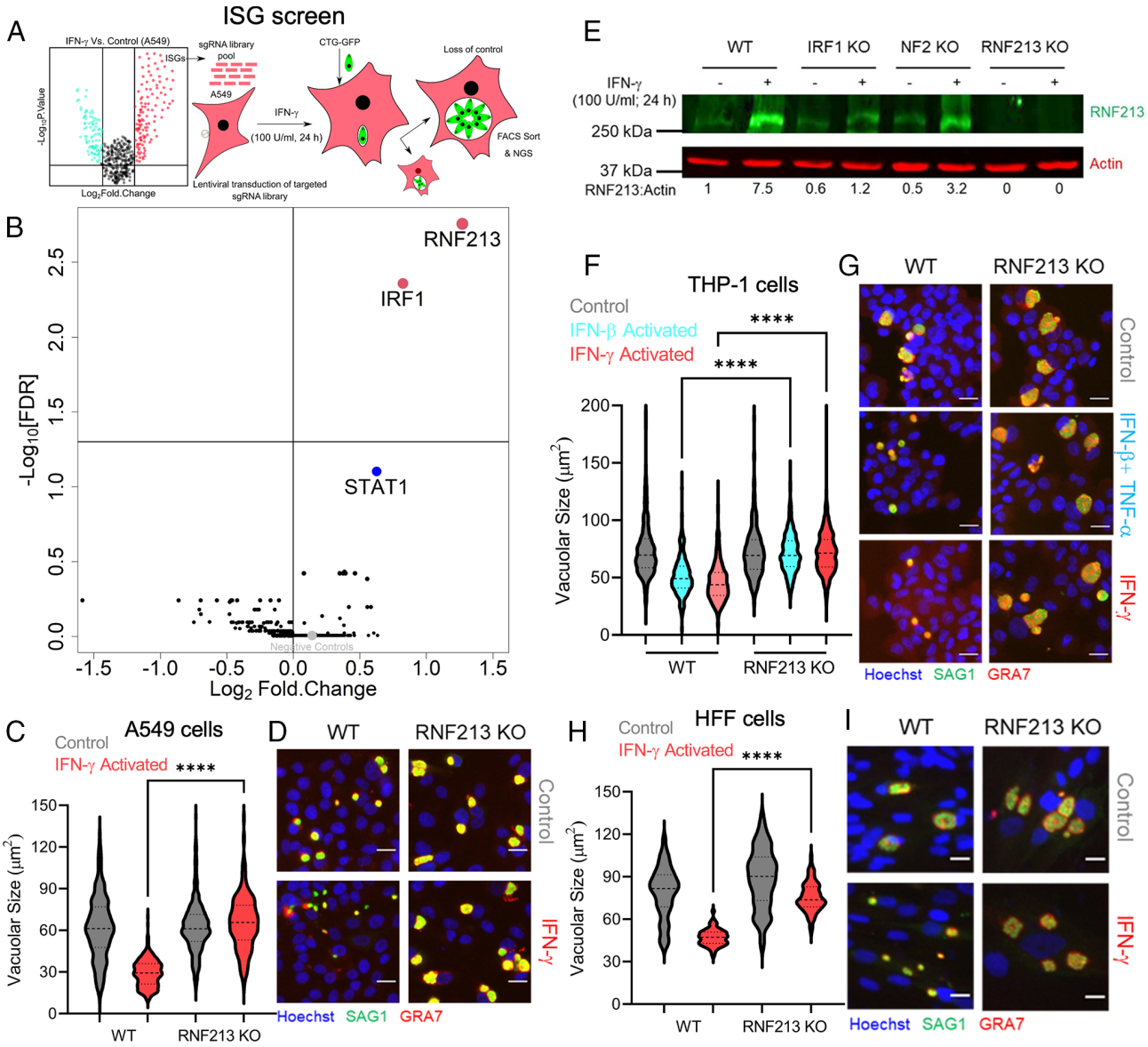

Fig. 3. CRISPR-Cas9 screen identifies RNF213 as required for IFN-γ-mediated growth restriction. (*A*) ISG-targeted sgRNA CRISPR-Cas9 screen using a subpool of ISGs up-regulated in IFN-γ-treated A549 cells (31). (*B*) Targeted sgRNA screen of ISGs up-regulated by IFN-γ identified two genes that were significantly depleted in the top 5% of CTG-GFP expressing cells (red). Log_2 fold change is plotted against $-log_{10}$ FDR for all four independent replicates combined. *STAT1* (blue) is marked to identify one of the positive controls for the screen. (*C*) WT and RNF213 KO A549 cells (*SI Appendix*, Fig. S3*C*) treated ± IFN-γ (100 U/mL) for 24 h, infected with CTG strain *T. gondii*, and evaluated for growth restriction by quantifying vacuolar size. Vacuolar growth was measured for at least three independent biological replicates with 30 images per sample. The violin plot shows mean vacuolar size per image. ****$P < 0.01$ using two-tailed unpaired Student's *t* test with Welch's correction. (*D*) Staining: nuclei Hoechst (blue), parasites anti-SAG1 (green), and vacuoles anti-GRA7 (red). (Scale bar, 20 μ.) (*E*) Cell lysates were immunoblotted using anti-RNF213 antibody, and the intensity was normalized to actin as loading control. (*F*) Vacuolar growth of parasites at 40 hpi in control and treated RNF213 KO human THP-1 macrophages (*SI Appendix*, Fig. S3 *D* and *E*). The violin plot shows mean vacuolar size ($μm^2$) per image for at least three biological replicates with at least 30 images per sample. Statistical analysis: ****$P < 0.0001$ using one-way ANOVA with Tukey's multiple comparisons test. (*G*) Representative images of control and treated cells infected with CTG and analyzed at 40 hpi. Staining: nuclei Hoechst (blue), parasites anti-SAG1 (green), and vacuoles anti-GRA7 (red). (Scale bar, 20 μ.) (*H*) Vacuolar growth of parasites at 40 hpi in ± IFN-γ-activated WT and RNF213 KO HFF cells (*SI Appendix*, Fig. S3*F*). The violin plot shows mean vacuolar size ($μm^2$) per image for at least three independent biological replicates with at least 30 images per sample. Statistical analysis:****$P < 0.0001$, two-tailed unpaired Student's *t* test with Welch's correction. (*I*) Representative images of the vacuole size in control and IFN-γ-activated WT and RNF213 KO HFF cells infected with CTG and analyzed at 40 hpi. Staining: nuclei Hoechst (blue), parasites anti-SAG1 (green), and vacuoles anti-GRA7 (red). (Scale bar, 20 μ.)

genome-wide screen (Dataset S1), and it narrowly missed the significance criteria for the secondary pool screen, although sgRNA guides for this gene were enriched in the top 5% population in 3 of 4 replicates by >twofold. Given its prominent position in the targeted ISG screen, we decided to examine its function. Deletion of *RNF213* (*SI Appendix*, Fig. S3*C*) resulted in enhanced growth of CTG strain parasite in untreated cells, and it completely reversed the growth inhibition normally seen in IFN-γ-treated A549 cells (Fig. 3 *C* and *D*). Moreover, the expression of RNF213 was decreased by ~ 50% in IRF-1 KO and NF2 KO cells treated with IFN-γ (Fig. 3*E*), suggesting that they both act through this downstream mediator. Notably, although sgRNAs were present for several mediators that have previously been found to play a role in restricting *T. gondii* growth [i.e., *IDO1* (22), *ISG15* (25), *GBP1* (29), and *RARRES3* (31)], their frequencies were not changed in the top 5% pool, indicating that the singular loss of these genes does not contribute substantially to IFN-γ-mediated growth restriction under the conditions of the screen.

To test how widely conserved the function of RNF213 was, we generated KOs in the human monocytic cell line THP-1 (*SI Appendix*,

Fig. S3 *D* and *E*) and human foreskin fibroblasts (HFF) (*SI Appendix*, Fig. S3*F*). Similar to A549 cells, loss of RNF213 in THP-1 cells reversed the inhibition of *T. gondii* growth following treatment with either IFN-γ or IFN-β combined with TNF-α (Fig. 3 *F* and *G*), treatments that have previously been shown to control *T. gondii* growth (7). Additionally, the loss of RNF213 resulted in slightly enhanced growth in untreated HFF cells and a loss of IFN-γ-mediated growth inhibition (Fig. 3 *H* and *I*). Notably, the loss of RNF213 in all three cell types completely reversed the effects of IFN-γ, similar to loss of STAT1 or IRF-1 in A549 cells. Additionally, RNF213 was involved in IFN-γ-mediated restriction of type I RH (*SI Appendix*, Fig. S3*G*) and type II ME49 (*SI Appendix*, Fig. S3 *H* and *I*) strains of *T. gondii*. Collectively, these findings argue that RNF213 is the major effector downstream of both type I and type II IFNs that inhibits *Toxoplasma* growth in human cells.

RNF213 Participates in Interferon-Mediated Control of Bacterial and Viral Pathogens. Previous studies have described a role for RNF213 in recognition and ubiquitination of LPS on intracellular *Salmonella* (36). To explore the role of RNF213 in control of intracellular bacteria that do not contain LPS, we examined the requirement for RNF213 in IFN-γ-activated A549 cells infected with *Mycobacterium tuberculosis* (Mtb). As expected, the colony forming units (CFU) of Mtb remained static in IFN-γ-treated cells grown for 48 h, compared to control cells where they increased significantly (Fig. 4*A*). Loss of RNF213 significantly impaired the ability of IFN-γ to control replication of Mtb (Fig. 4*A*). Immunofluorescence localization also revealed that RNF213 was recruited to the surface of Mtb in A549 cells and that these vacuoles also stained with FK2, an antibody that recognizes monoubiquitin and polyubiquitin chains (37) (Fig. 4*B*). RNF213 has also been reported to facilitate control of Rift Valley fever virus, an enveloped segmented RNA virus (38). We also explored the potentially broad antimicrobial role of RNF213 in control of intracellular viral replication using a nonsegmented RNA virus. We examined type I IFN (IFN-β)-treated A549 cells infected with vesicular stomatitis virus expressing GFP (VSV-GFP). Treatment with IFN-β resulted in a significant decrease in viral replication in WT cells that was reversed in IRF-1 KO and RNF213 KO cells (Fig. 4 *C* and *D*). Taken together, these findings suggest that RNF213 may recognize a component that is common to multiple pathogens, rather than a panoply of different molecules each unique to specific pathogens.

Despite previous reports showing a role for GBP1 in IFN-γ-mediated control of *T. gondii* (28, 29), our ISG-focused CRISPR screen in A549 cells did not identify any *GBP* genes significantly involved in growth restriction (*SI Appendix*, Fig. S4*A*). We considered that the screen may have missed a role for *GBP1* due to technical reasons. Therefore, we examined GBP1 recruitment to vacuoles containing type III CTG parasites in both A549 and THP-1 cells after treatment with IFN-γ. We did not detect GBP1 recruitment to the PVM (parasitophorous vacuole membrane) of type III CTG parasites in either cell type after IFN-γ treatment (*SI Appendix*, Fig. S4 *B* and *C*). To further confirm these findings, we generated *GBP1* knockout A549 and THP-1 cells using CRISPR/Cas9 (*SI Appendix*, Fig. S4*D*). Loss of GBP1 did not affect the ability of IFN-γ to restrict the growth of type III CTG strain parasites in either A549 (*SI Appendix*, Fig. S4*E*) or THP-1 cells (*SI Appendix*, Fig. S4*F*). Additionally, we investigated whether growth restriction following treatment with IFN-γ resulted in cell death, as previously reported in infected THP-1 cells (39). However, we did not observe any significant increase in cell death following IFN-γ activation of either WT or GBP1 KO THP-1 cells infected with type III CTG strain parasites (*SI Appendix*, Fig. S4*G*).

RNF213-Dependent Growth Restriction Leads to Recruitment of Autophagy Adaptors but Is Independent of ATG5. Consistent with its requirement for growth restriction, RNF213 was recruited to a portion of *T. gondii* vacuoles in untreated cells, and this

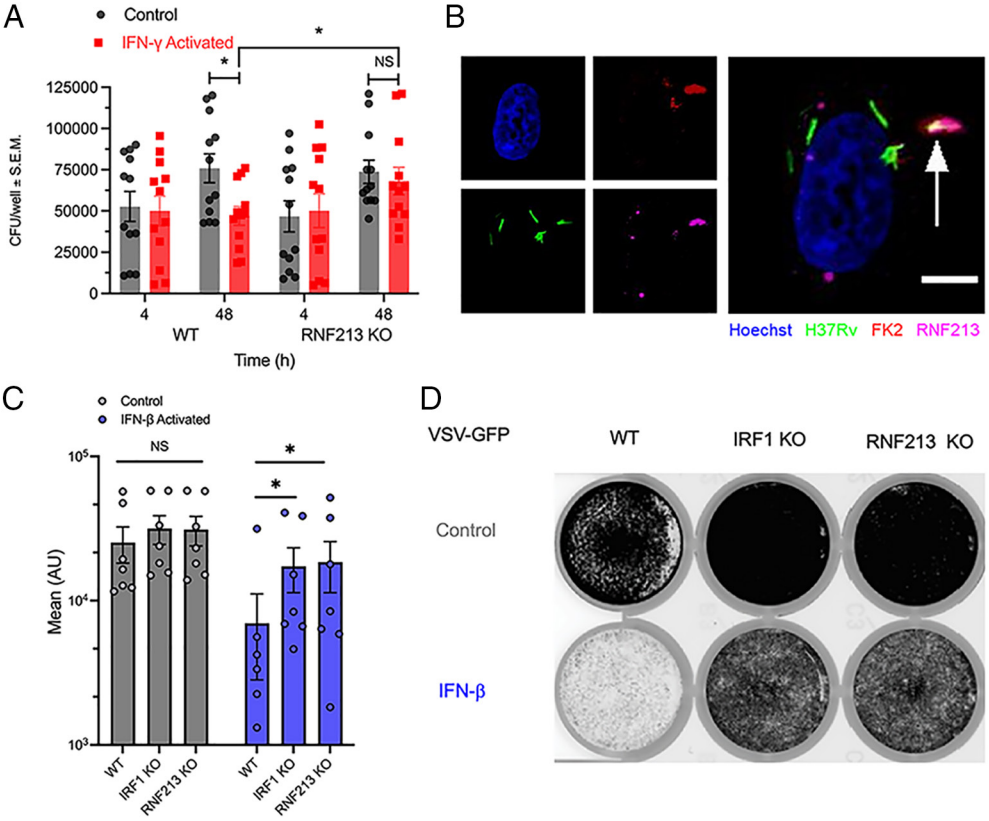

Fig. 4. RNF213 is required for interferon-mediated control of intracellular bacterial and viral infection in human cells. (*A*) Mtb growth in ± IFN-γ (100 U/mL for 24 h) activated WT and RNF213 KO A549 cells at 4 and 48 hpi. Data show mean CFU per well ±SEM from four independent experiments each with three internal replicates. Statistical analysis: $^*P < 0.05$ using two-tailed unpaired Student's *t* test. (*B*) Representative image showing colocalization of Mtb (green) with ubiquitin and RNF213. Cells were stained with FK2 (red) and RNF213 (magenta) in IFN-γ-activated A549 cells that were analyzed at 8 hpi. The arrow depicts FK2 positive and RNF213 positive Mtb. Nuclei are labeled with Hoechst (blue). (Scale bar, 5 μ.) (*C*) Control and IFN-β (24 h, 100 U/mL) activated WT, IRF1 KO, and RNF213 KO A549 cells infected with MOI 1 VSV-GFP (recombinant VSV expressing enhanced green fluorescent protein) at 24 hpi. The bar plot shows levels of GFP expression plotted as mean arbitrary units (AU). Data are means ± SEM for seven independent biological replicates. Statistical analysis: $^*P < 0.05$ using two-way ANOVA with Dunnett's multiple comparison test. (*D*) Representative images showing total GFP emission imaged by Typhoon scanning of the 24-well plate.

increased dramatically following treatment with IFN-γ as shown by immunofluorescence assay and immuno-EM (Fig. 5 *A*–*C*). Since ubiquitination is thought to be the first step in marking the *T. gondii* vacuole for growth restriction (24), we stained cells with FK2, which recognizes both mono- and polyubiquitin (Ub) chains, in combination with RNF213. The proportion of vacuoles that were FK2 positive closely matched the percentage that were also positive for RNF213, while the number that were RNF213 positive considerably exceeded this value (Fig. 5*C*). The higher percentage of RNF213-positive staining vacuoles suggested that RNF213 is initially recruited to the PVM followed by ubiquitination, resulting in double-positive vacuoles. Similar costaining of RNF213 and FK2 was observed in IFN-γ-activated HFF and THP-1 cells infected with CTG (*SI Appendix*, Fig. S5 *A* and *B*). Vacuoles containing the type I RH strain were also positive for RNF213 and FK2 in IFN-γ-activated WT A549 cells, whereas vacuoles in the RNF213 KO uniformly lacked staining of FK2 (*SI Appendix*, Fig. S5 *C* and *D*). Likewise, the majority of vacuoles containing the type II PRU strain showed staining of RNF213 and FK2 in WT A549 cells and FK2 staining was dramatically decreased in the RNF213 KO (*SI Appendix*, Fig. S5 *E* and *F*). Interestingly, a subset (i.e., 5 to 10%) of vacuoles containing type II PRU parasites showed RNF213-independent FK2 staining in both WT and RNF213 KO A549 cells (*SI Appendix*, Fig. S5 *E* and *F*). Downstream of IFN-γ-mediated ubiquitination, the PVM acquires several adaptors, including p62 and NDP52, that recruit the autophagy adaptor LC3 (24–26). Consistent with these previous reports, recruitment of LC3 was low in nonactivated cells and significantly elevated after treatment with IFN-γ (Fig. 5 *D* and *E*). The proportion of vacuoles that were positive for both FK2 and LC3 was similar, while singly FK2-positive vacuoles considerably exceeded this value (Fig. 5*E*). These differences in positivity suggest that ubiquitination occurs first, followed by recruitment of LC3. Although the parasites were positive for LC3, they were not associated with either acidified compartments (Lysotracker) or LAMP1, both of which act as a marker for lysosomes inside the cell (*SI Appendix*, Fig. S6 *A*–*C*).

Examination of the vacuole membrane surrounding the parasite by transmission electron microscopy revealed that it was often wrapped by numerous membranes (Fig. 5*F*), a phenotype that has previously been associated with growth restriction by noncanonical autophagy (24). Combined with the recruitment LC3, this profile suggested that RNF213 may act to recruit components of the noncanonical autophagy pathway to restriction growth of the parasite. To test this idea, we generated a knockout of *ATG5* in A549 cells and verified its absence by western blotting and loss of conversion of LC3I to the lipidated LC3II form (Fig. 5*G*). Contrary to expectation, loss of ATG5 minimally affected the growth restriction of *T. gondii* in IFN-γ-treated cells (Fig. 5*H*). To ascertain whether loss of ATG5 might have affected the recruitment of RNF213 to the parasite containing vacuole, we stained IFN-γ-treated and infected ATG5 KO cells for RNF213 and FK2. Similar to WT cells, parasites were frequently labeled by both RNF213 and FK2 in ATG5 KO cells (Fig. 5*I*). Collectively, these findings indicate that RNF213 lies upstream of ubiquitination and that growth restriction requires RNF213 but is ATG5 independent.

Recruitment of RNF213 to the Vacuole Initiates *Toxoplasma* Restriction. RNF213 is an E3 ubiquitin ligase that is recruited to the *Salmonella* containing vacuole where it ubiquitinylates the lipid A moiety of LPS (36). Mutation in the AAA+ ATP hydrolysis (E2845A) and E3 RZ-finger (H4509A) domains abrogated RNF213 recruitment to the *Salmonella* vacuole and thus prevented it from ubiquitinating LPS (36). We therefore tested the requirement of these same residues in RNF213 recruitment and ubiquitination of the *Toxoplasma* PVM in A549 cells. RNF213 KO cells (*SI Appendix*, Fig. S7*A*) were complemented with mCherry tagged WT, E2845A, or H4509A variants of RNF213 (*SI Appendix*, Fig. S7*B*). The cells were activated with IFN-γ activation, infected with CTG-GFP, and assessed for recruitment, ubiquitination, and growth restriction. WT mCherry-RNF213 was strongly recruited to vacuoles containing CTG-GFP parasites at 6 hpi resulting in efficient ubiquitination (FK2 staining) (Fig. 6 *A* and *B*). Similar to *Salmonella*, complementation with E2845A mCherry-RNF213 failed to be recruited to the vacuole (Fig. 6 *A* and *B*). Complementation with H4509A mCherry-RNF213 resulted in partial reduction in recruitment to vacuoles containing CTG-GFP parasites (Fig. 6 *A* and *B*). Interestingly, all the H4509A mCherry-RNF213-positive parasite containing vacuoles were nonubiquitinated (FK2 negative), confirming that this residue is needed for ubiquitin transfer or ubiquitination initiation (36) (Fig. 6 *A* and *B*). Time-lapse microscopy of the WT mCherry-RNF213 complemented line showed that recruitment starts at 2 hpi and envelopes the vacuole within 15 to 20 min (Fig. 6*C* and Movie S1). We then assess growth restriction in complemented cells using the vacuole size assay described above. Complementation with WT mCherry-RNF213 (WT RNF213) showed significant restriction of parasite growth under IFN-γ activation in comparison to RNF213 KO cells (Fig. 6 *D* and *E*). Interestingly, complementation with WT mCherry-RNF213 also significantly inhibited growth of CTG parasites under nonactivated conditions in comparison to WT cells (Fig. 6 *D* and *E*). These results indicate that RNF213 is both necessary for growth restriction following IFN-γ activation and is also sufficient to impair growth even in the absence of activation. Finally, complementation with the mCherry-E2845A-RNF213 or mCherry-H4509A -RNF213 mutants failed to restore growth restriction, indicating that both recruitment and ubiquitination are necessary for the activity of RNF213 in pathogen control.

Discussion

To identify conserved mechanisms of cell-autonomous immunity to intracellular pathogens, we performed a genome-wide CRISPR screen for loss of *T. gondii* growth restriction in response to IFN-γ. Although the primary screen failed to identify previous candidate genes implicated in control, we ascribed a role for the tumor suppressor gene *NF2* in up-regulating expression of IRF-1-dependent ISGs. To account for the possibility that the primary screen lacked power to identify single gene effects, we performed an ISG-targeted screen for loss of IFN-γ-mediated *T. gondii* growth restriction. The ISG-targeted screen identified the E3 ligase *RNF213* as the primary effector important for IFN-γ-mediated control of *T. gondii* growth in human cells. RNF213 was up-regulated by IFN-γ, recruited to the parasite containing vacuole, and associated with initial ubiquitination of targets at this interface. Deletion of *RNF213* revealed that it was necessary for growth restriction, despite not relying on ATG5, which may act at downstream steps independent of growth restriction. Moreover, overexpression of RNF213 led to growth restriction even in the absence of IFN-γ, indicating that it operates independently of other ISGs. Loss of RNF213 also diminished antibacterial and antiviral responses to interferon, suggesting that it controls a common host pathway needed for pathogen resistance in human cells.

To provide an unbiased method to identify genes important for IFN-γ-mediated control of *T. gondii*, we developed a FACS-based CRISPR-screen to identify genes whose absence results in loss of IFN-γ-mediated growth restriction. The genome-wide CRISPR

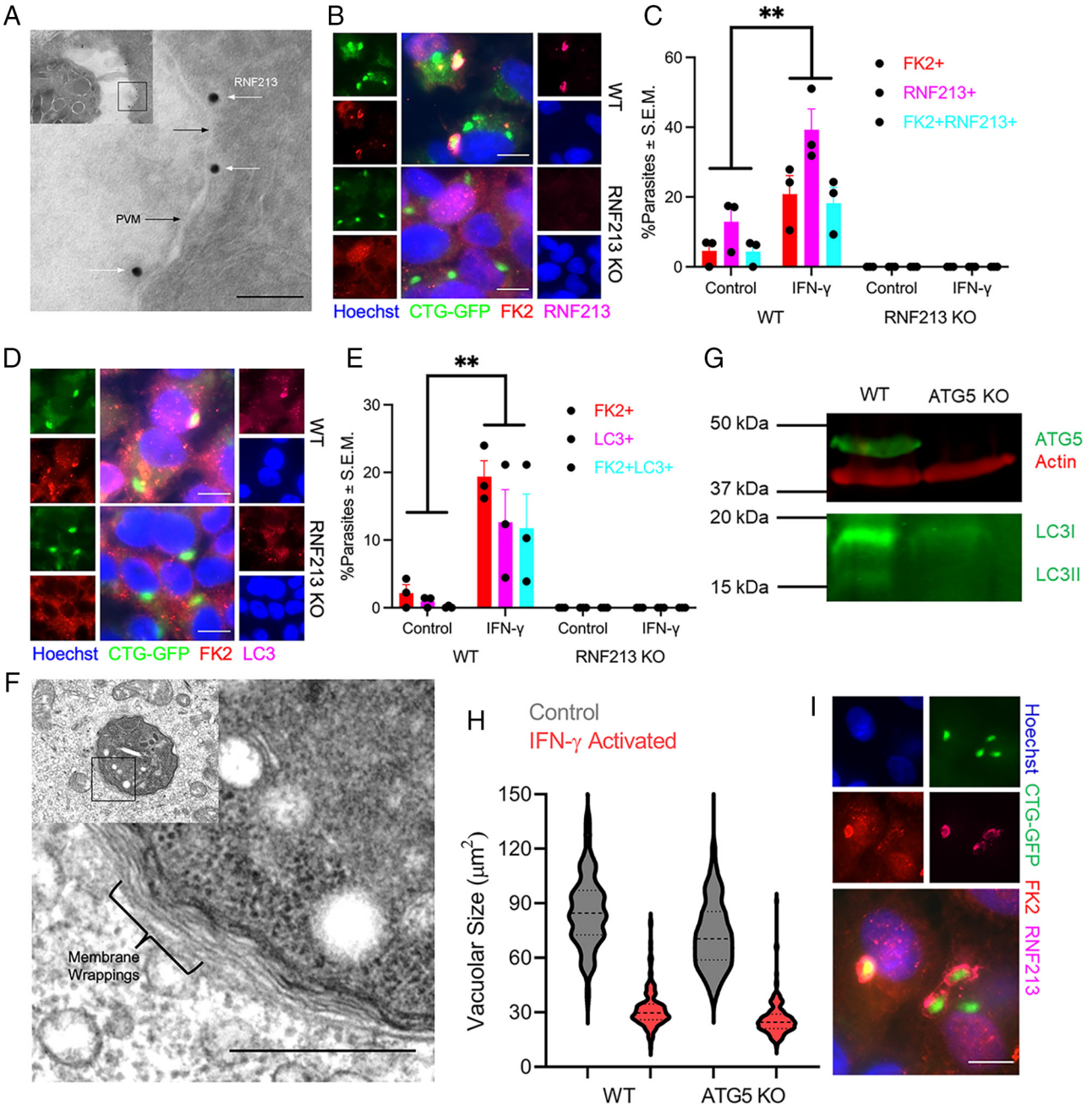

Fig. 5. RNF213 colocalized with ubiquitinated parasite-containing vacuoles. (*A*) Immuno-EM labeling of RNF213 in IFN-γ-activated WT A549 cell infected with CTG parasite (*Inset*) at 6 hpi. Parasitophorous vacuolar membrane (PVM). (Scale bar, 100 nm.) (*B*) Representative images of WT and RNF213 KO A549 cells infected with CTG-GFP at 6 hpi. Staining: FK2 (mono-polyubiquitin; red), anti-RNF213 (magenta), nuclei Hoechst (blue), and GFP parasites (green), (Scale bar, 10 μ.) (*C*) Quantification of FK2+ (red), RNF213+ (magenta), and FK2+RNF213+ (cyan) parasites for at least three biological replicates, mean ± SEM. Statistical analysis: $^{**}P < 0.01$ using two-way ANOVA with Tukey's multiple comparisons test. (*D*) Representative images of WT and RNF213 KO A549 cells infected with CTG-GFP at 6 hpi. Staining: FK2 (red), anti-LC3B (magenta), nuclei Hoechst (blue), and GFP parasites (green). (Scale bar, 10 μ.) (*E*) Quantification of FK2 positive (red), LC3 positive (magenta), and FK2 positive LC3 positive (cyan) parasites for at least three biological replicates, mean ± SEM. $^{**}P < 0.01$ using two-way ANOVA with Tukey's multiple comparisons test. (*F*) Transmission electron microscopic image of IFN-γ-activated WT A549 cell infected with CTG parasite (*Inset*) at 6 hpi. Membrane wrapping is highlighted in the magnified view. (Scale bar, 500 nm.) (*G*) ATG5 (*Top*) and LC3B (*Bottom*) immunoblots of WT and ATG5 KO A549 cells. Actin was used as loading control. (*H*) Vacuolar growth of CTG parasite at 40 hpi in ± IFN-γ-activated WT and ATG KO cells. The violin plot shows mean vacuolar size (μm^2) per image for at least three independent biological replicates with at least 30 images per sample. (*I*) Representative image of IFN-γ-activated ATG5 KO A549 cells infected with CTG-GFP at 6 hpi. Staining: FK2 (red) and anti-RNF213 (magenta). (Scale bar, 10 μ.)

screen identified several components in the STAT1 signaling pathway including *JAK2*, the receptors *IFNGR1* and *IFNGR2*, and the transcription factor *IRF-1*. Consistent, with the ability of IRF1 to up-regulate many ISGs (40), we found that IRF-1 was necessary for maximal growth control following IFN-γ stimulation. Independently, we have previously shown that overexpression of IRF-1 in A549 cells is sufficient to induce control of *T. gondii* growth (31). We also identified *NF2* as a significant hit in the primary genome-wide and pooled secondary CRISPR screens. Deletion of *NF2/Merlin* significantly reduced the expression of IFN-γ-induced, IRF-1-dependent genes by ~ 25%, in addition to dysregulating numerous unrelated genes. This finding was unexpected as *NF2* is known as a tumor suppressor gene that negatively regulates mTOR and the Hippo signaling pathways (41, 42). Although it is without prior connection to interferon signaling, our finding indicates that it modulates IRF-1-dependent gene

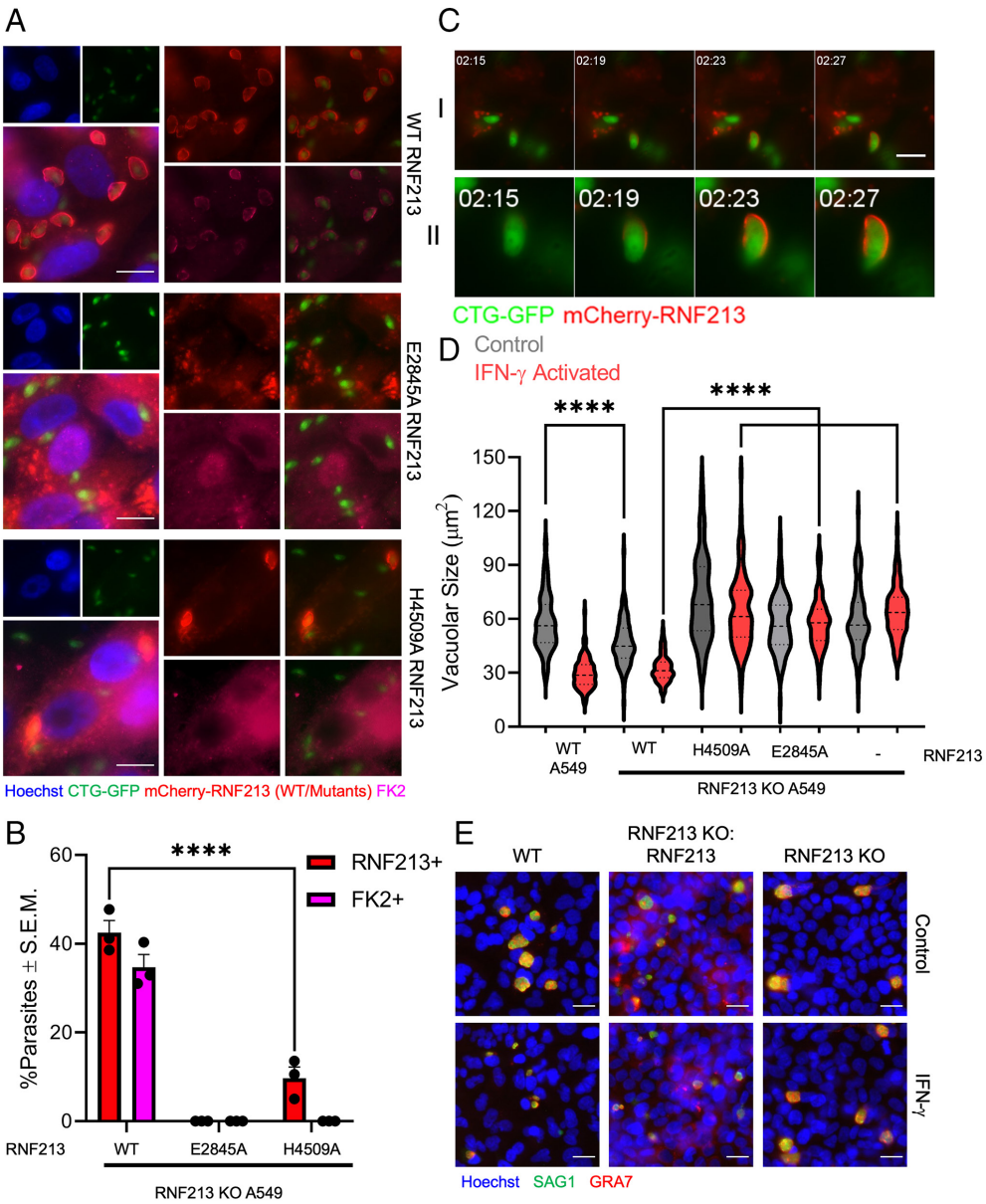

Fig. 6. RNF213 recruitment restricts *Toxoplasma*. (*A*) mCherry tagged WT, E2845A (ATPase mutant) and H4509A (RZ finger histidine mutant) RNF213 isoforms (red) were complemented into RNF213 KO A549 cells. The cells were activated with IFN-γ (100 U/mL; 24 h), infected with CTG-GFP, and analyzed at 6 hpi. Staining: FK2 (magenta), nuclei Hoechst (blue), and GFP parasites (green). (Scale bar, 10 μ.) (*B*) Quantification of RNF213-positive (mCherry; red) and FK2-positive (magenta) parasites for at least three biological replicates, mean ± SEM. ****$P < 0.0001$ using two-way ANOVA with Tukey's multiple comparisons test. (*C*) Time-lapse imaging of *Toxoplasma* infection (CTG-GFP; green) in IFN-γ-activated (100 U/mL, 24 h) mCherry-RNF213 (red) expressing RNF213 KO A549 cells. Row II magnified of row I. (Scale bar, 10 μ.) (*D*) WT, RNF213 KO, complemented lines of A549 cells treated ± IFN-γ (100 U/mL) for 24 h, infected with CTG strain *T. gondii*, and evaluated for growth restriction at 40 hpi. The violin plot shows mean vacuolar size (μm^2) per image for at least three independent biological replicates for at least 30 images per sample. Statistical analysis: ****$P < 0.0001$, one-way ANOVA with Sidak's multiple comparison test. (*E*) Representative images of control and IFN-γ-activated WT, RNF213 KO, and complemented A549 cells at 40 hpi. Staining: nuclei Hoechst (blue), parasites anti-SAG1 (green), and vacuole anti-GRA7 (red). (Scale bar, 10 μ.)

expression. Among the ISGs that are NF2 and IRF-1 dependent, RNF213 may factor prominently given its essential downstream role in IFN-γ-mediated growth inhibition.

Both genome-wide CRISPR and targeted ISG screens failed to find previous candidate genes including *RARESS3* (31), *ISG15* (25), *GBP*s (29, 30), and *IDO1* (22). Hence, while these genes have demonstrable effects when tested individually, their contributions were too modest to show differences at the population level, at least based on the conditions used here. Our failure to identify GBP1 as a restriction factor in the CRISPR screens was particularly surprising, given its previous role in restricting *T. gondii* growth in both A549 and THP-1 cells (28, 39). Additionally, direct knockout of this gene in A549 and THP-1 cells did not reveal a contribution to IFN-γ-mediated restriction. This difference may be due to the multiplicity of infection (MOI) that we purposefully kept low (i.e., <1) in our growth assays, due to the fact that high MOI with type I (RH) and II (PRU) parasites causes nonspecific cell death in murine bone marrow-derived macrophages (43). Instead of these previously characterized factors, the ISG-targeted CRISPR screen identified a prominent role for RNF213, which is expressed at basal levels and up-regulated in response to IFN-γ (31). RNF213 was essential for IFN-γ-mediated restriction of *T. gondii* growth in multiple human cell types and against multiple strain types, making it a broadly acting restriction factor.

We observed that RNF213 was recruited to a proportion of parasite containing vacuoles even in unstimulated cells, consistent with the fact that it is expressed at basal levels yet induced by IFN-γ. Similarly, RNF213 is recruited to vacuoles containing intracellular

Salmonella (36), *Listeria* (44), and *Chlamydia* lacking the effector GarD (45), and to restrict their growth in the absence of IFN-γ stimulation. There was a significant increase in the growth of *T. gondii* in nonstimulated cells lacking RNF213, and overexpression of mCherry-RNF213 also led to growth restriction in the absence of IFN-γ activation, indicating that it is sufficient to impart growth restriction in the absence of other ISGs. Notably, RNF213 was recruited early during infection and was associated with ubiquitination of yet unknown targets on the parasite containing vacuole. Importantly, unlike type I and III Toxoplasma parasites, some type II PRU parasites became ubiquitinated independently of RNF213. This result suggests the presence of an additional ubiquitin ligase for type II parasites in addition to RNF213. Type II PRU parasites express a form of GRA15 that recruits human E3 ligases TRAF2 and TRAF6 (46) and activates downstream NF-kB signaling (47). Hence, it will be interesting in future studies to test the involvement of these and other E3 ligases in regulating ubiquitination of different parasite strains. RNF213 was present on the PVM before autophagy marker LC3, and notably, its presence on the vacuole did not rely on ATG5. Moreover, the growth restriction imparted by IFN-γ treatment was largely independent of ATG5 and yet fully dependent on RNF213. Taken together, these finding suggest a model whereby RNF213 is initially recruited to the parasite-containing vacuole where it ubiquitinates unknown targets leading to growth restriction. Our data also indicate that the canonical ATG pathway is not required for growth restriction, although it may be important in downstream events such as antigen processing.

The mechanism by which RNF213 is loaded on to pathogen containing vacuoles remains undefined; however, based on the E2845A mutant, its ATPase activity is required for recruitment to both *T. gondii* and *Salmonella* vacuoles. In contrast to *Salmonella,* the H4509A RNF213 mutant protein was still recruited to *Toxoplasma* vacuoles, albeit with a reduced frequency vs. WT RNF213. Despite recruitment, H4509A RNF213 failed to show any FK2 staining at the PVM, consistent with a requirement for the C-terminal RZ-finger domain in ubiquitylation (36). Importantly, neither of the RNF213 mutants were able to recover growth inhibition, indicating that both recruitment and ubiquitination are required for the function of RNF213.

The broad activity of RNF213 against multiple different pathogens suggests that there may be some common determinant recognized by its multiple domain structure that includes a dynein-like core with 6 ATPase units and a multidomain E3 module (48). Previous studies have demonstrated that LPS on cytoplasmic *Salmonella* is targeted by RNF213-mediated ubiquitination (36), although the exact chemical adduct remains to be defined. However, other pathogens including intracellular *Listeria*, and various viruses that have been shown to be targeted by RNF213 (44), lack LPS. The pathogens studied here also do not contain LPS, indicating that they must be recognized by a different mechanism. The broad nature of organisms targeted by RNF213 favors a model in which RNF213 recognizes a host target, either protein or lipid, whose modification leads to restricted pathogen growth. Future studies to elucidate this mechanism may enable enhanced cell-autonomous immunity to clear intracellular pathogens without the adverse effects of treatment with interferons.

Materials and Methods

Refer to supplementary materials and methods for descriptive methodology, primers, plasmids, key reagents, and parasites and cell lines (Datasets S4–S6). Vacuolar growth and luciferase-based (49) growth assays were performed as described in *SI Appendix*.

Cloning and Lentiviral Transduction of the sgRNA Libraries. A collection of sgRNAs for the ISG screen were designed using sgRNA designer at the Genetic Perturbation Platform web portal (https://portals.broadinstitute.org/gpp/public/analysis-tools/sgrna-design) and cloned into lentiCRISPR v2 (Addgene, # 52961). These custom sgRNA libraries, along with the Brunello library (Addgene #73179), were electroporated into Endura electrocompetent cells (Lucigen Bioresearch Technologies) at >100X coverage. Subsequently, the libraries were packaged in 293T cells by cotransfection with pRSV-Rev (Addgene # 12253), pMD2.G (Addgene # 12259), and pMDLg/pRRE (Addgene # 12251), followed by transduction into A549 cells at >100X coverage.

FACS-Based CRISPR/Cas9 Screen. FACS-based CRISPR screens involved sorting of top 5% (T5) of 30 to 50 million library-transduced IFN-γ-activated A549 (+100 U/mL IFN-γ, 24 h) cells infected with CTG-GFP (MOI 0.5, 40 h) based on GFP intensity. Genomic DNA was isolated from sorted cells and uninfected control for each of four biological replicates per library followed by PCR of transduced sgRNAs. The PCR amplicons were barcoded, pooled, and sequenced on an Illumina NovaSeq-6000 with at least 100x coverage of 150 bp paired-end reads. Basecalls and demultiplexing were performed with Illumina's bcl2fastq2 software. The forward reads were analyzed using the MAGeCKFlute package (50) in R.

RNA Sequencing. Total RNA of A549 cells (±100 U/mL hIFN-γ, 24 h) from three independent biological replicates was extracted using the Qiagen RNeasy Mini Kit and sequenced on an Illumina NovaSeq-6000 to generate paired-end reads extending 150 bases. Basecalls and demultiplexing were performed with Illumina's bcl2fastq2 software. The fastq files were imported into CLC Genomics Workbench version 21.0.5 (QIAGEN Bioinformatics, Inc.) to map against hg38 reference genome. The gene expression data were imported into R to generate heat map of differentially expressed genes and compare RPKM values of ISGs across samples.

CRISPR-Cas9-Mediated Gene Deletions and Piggybac Complementation. sgRNAs were cloned into lentiCRISPR v2 and packaged with pRSV-Rev, pMD2.G, and pMDLg/pRRE in 293T cells. Virus containing supernatant was transduced into different cell lines and selected with puromycin. Single cell knockouts were FACS sorted, validated via western blotting, and Sanger sequencing. A549 RNF213 KO line was generated by transfecting px458 (Addgene, # 48138) plasmid with RNF213 sgRNA. RNF213 complemented cells were made by cotransfecting piggybac-RNF213 plasmids (encoding WT, E2845A and H4509A) with super piggybac transposase vector (System Biosciences) into RNF213 KO A549 cells. Selection involved 2 wk in 1 mg/mL G418 (Geneticin, Thermo Fisher Scientific).

ISRE Promoter Assay. The cells were cotransfected with 50 ng of plasmid expressing ISRE reporter (7) and 50 ng of pCMV-Red Firefly Luc Vector (Thermo Fisher Scientific) using lipofectamine LTX. Twenty-four hours after transfection, cells were treated with ±100 U/mL hIFN-β for another 24 h. Gaussia luciferase activity was measured in the supernatant, and Firefly luciferase activity was measured in the cell lysates using the luciferase glow assay kits (Thermo Fisher Scientific).

Immunofluorescence Staining. Cells (±100 U/mL hIFN-γ, 24 h) were seeded onto 12-mm coverslips in a 24-well plate, infected with CTG-GFP (MOI 3, 6 h), fixed with 4% paraformaldehyde, blocked with 5% FBS+5% normal goat serum, and stained with FK2 (1:2,000), anti-RNF213 (1:2,000), anti-GBP1 (1:2,000) and/or anti-LC3 (1:2,000). Cells were then stained with Alexa-Fluor conjugated secondary antibodies and Hoechst to stain nuclei (Life Technologies).

Time-Lapse Microscopy. mCherry tagged RNF213 complemented A549 cells (+100 U/mL hIFN-γ) were seeded overnight on MatTek 25 mm dishes, infected with CTG-GFP (MOI 3, 2 h), washed 2 hpi, and imaged using a AxioObserver equipped with Heating Unit XL S (Zeiss) at 37 °C and 5% CO_2.

***M. tuberculosis* and VSV Infection.** *M. tuberculosis* (Mtb) were used to infect A549 cells (±100 U/mL hIFN-γ) at MOI 0.5 for 4 h followed by washing to remove extracellular bacteria. For CFUs, infected cells were lysed in 0.06% SDS solution and plated on 7H11 agar plates (BD Biosciences, # 283810) containing OADC (BD Biosciences, # 212351) and glycerol. For microscopy, H37Rv-GFP-infected cells were fixed at 8 hpi with 4% paraformaldehyde for 1h, permeabilized, and blocked in PBS with 0.05% Triton X-100 and 3% BSA. The cells were stained with FK2 (1:2,000) and anti-RNF213 (1:2,000) overnight at 4 °C followed by Alexa-Fluor conjugated secondary antibodies with Hoechst to stain nuclei.

For VSV infections, A549 cells (±100 U/mL hIFN-β) were infected with VSV-GFP at MOI 1 for 24 h. GFP intensity was determined by scanning cells with an Amersham Typhoon 5 imager (GE) and images quantified by ImageJ.

Cell Death Assay. WT and GBP1 KO THP-1 cells (±100 U/mL hIFN-γ) infected with CTG parasites (MOI 0.5, 2 h) were stained with 2 μM ethidium homodimer-2 (Thermo Fisher Scientific) in PBS for 30 min at 2 h and 24 h postinfection. Ethidium homodimer–positive nuclei were measured as a percentage of total nuclei after fixation with 4% paraformaldehyde and parasite staining.

Statistical Analysis. Statistical analysis for each experiment was performed on the combined data in PRISM (GraphPad). Replicates, significance values, and tests performed are included in the figure legends.

Data, Materials, and Software Availability. RNASeq data have been submitted to GEO under accession number GSE215771 (51).

ACKNOWLEDGMENTS. We thank Dr. Wandy Beatty, Microbiology Imaging Facility, Washington University in St. Louis, for performing the electron microscopy studies. We also thank Jennifer Barks for cell culture support, members of the Sibley lab for helpful comments, Robert Orchard for advice on the CRISPR screens, and Felix Randow for communications prior to publication. The plasmid expressing mCherry tagged RNF213 was a kind gift from Dr. Daisuke Morito. This work was supported in part by grants from the NIH (AI154048 and AI118426).

Author affiliations: [a]Department of Molecular Microbiology, School of Medicine, Washington University in St. Louis, St Louis, MO 63130; [b]Department of Medicine, Division of Infectious Diseases, School of Medicine, Washington University in St. Louis, St Louis, MO 63130; and [c]Broad Institute of Harvard and Massachusetts Institute of Technology, Cambridge, MA 02142

Author contributions: S.K.M., H.P.K., P.C., J.A.P., S.D., and L.D.S. designed research; S.K.M., H.P.K., and P.C. performed research; A.B. and J.G.D. contributed new reagents/analytic tools; S.K.M., H.P.K., P.C., J.A.P., and S.D. analyzed data; and S.K.M. and L.D.S. wrote the paper.

1. L. D. Sibley, Invasion and intracellular survival by protozoan parasites. *Immunol. Rev.* **240**, 72–91 (2011).
2. I. A. Khan, M. Moretto, Immune responses to Toxoplasma gondii. *Curr. Opin. Immunol.* **77**, 102226 (2022).
3. E. M. Frickel, C. A. Hunter, Lessons from Toxoplasma: Host responses that mediate parasite control and the microbial effectors that subvert them. *J. Exp. Med.* **218**, e20201314 (2021).
4. G. S. Yap, A. Sher, Effector cells of both nonhemopoietic and hemopoietic origin are required for interferon (IFN)–gamma- and tumor necrosis factor (TNF)-alpha- dependent host resistance to the intracellular pathogen, *Toxoplasma gondii*. *J. Exp. Med.* **189**, 1083–1091 (1999).
5. Y. Suzuki, M. A. Orellana, R. D. Schreiber, J. S. Remington, Interferon-g: The major mediator of resistance against *Toxoplasma gondii*. *Science* **240**, 516–518 (1988).
6. S. J. Han *et al.*, Internalization and TLR-dependent type I interferon production by monocytes in response to Toxoplasma gondii. *Immunol. Cell Biol.* **92**, 872–881 (2014).
7. S. K. Matta *et al.*, *Toxoplasma gondii* effector TgIST blocks type I interferon signaling to promote infection. *Proc. Natl. Acad. Sci. U.S.A.* **116**, 17480–17491 (2019).
8. S. Mostafavi *et al.*, Parsing the interferon transcriptional network and its disease associations. *Cell* **164**, 564–578 (2016).
9. I. Rusinova *et al.*, Interferome v2.0: An updated database of annotated interferon-regulated genes. *Nucleic Acids Res.* **41**, D1040–D1046 (2013).
10. J. C. Howard, J. P. Hunn, T. Steinfeldt, The IRG protein-based resistance mechanism in mice and its relation to virulence in *Toxoplasma gondii*. *Curr. Opin. Microbiol.* **14**, 414–421 (2011).
11. R. T. Gazzinelli, R. Mendonca-Neto, J. Lilue, J. Howard, A. Sher, Innate resistance against Toxoplasma gondii: An evolutionary tale of mice, cats, and men. *Cell Host Microbe* **15**, 132–138 (2014).
12. J. D. MacMicking, Interferon-inducible effector mechanisms in cell-autonomous immunity. *Nat. Rev. Immunol.* **12**, 367–382 (2012).
13. Z. Zhao *et al.*, Autophagosome-independent essential function for the autophagy protein Atg5 in cellular immunity to intracellular pathogens. *Cell Host Microbe* **4**, 458–469 (2008).
14. J. Ohshima *et al.*, Role of mouse and human autophagy proteins in IFN-gamma-induced cell-autonomous responses against *Toxoplasma gondii*. *J. Immunol.* **192**, 3328–3335 (2014).
15. J. Choi *et al.*, The parasitophorous vacuole membrane of *Toxoplasma gondii* is targeted for disruption by ubiquitin-like conugation systems of autophagy. *Immunity* **40**, 924–935 (2014).
16. C. Hoffmann *et al.*, Evolving characteristics of toxoplasmosis in patients infected with human immunodeficiency virus-1: Clinical course and Toxoplasma gondii-specific immune responses. *Clin. Microbiol. Infect.* **13**, 510–515 (2007).
17. H. W. Murray, A. M. Granger, R. F. Teitelbaum, Gamma interferon-activated human macrophages and *Toxoplasma gondii*, *Chalmydia psittaci*, and *Leishmania donovani*: Antimicrobial role of limiting intracellular iron. *Infect. Immun.* **59**, 4684–4686 (1991).
18. C. F. Nathan, H. W. Murray, M. E. Weibe, B. Y. Rubin, Indentification of interferon gamma as the lymphokine that activates human macrophage oxidative metabolism and antimicrobial activity. *J. Exp. Med.* **158**, 670–689 (1983).
19. M. A. Orellana, Y. Suzuki, F. Araujo, J. S. Remington, Role of beta interferon in resistance to Toxoplasma gondii infection. *Infect. Immun.* **59**, 3287–3290 (1991).
20. J. L. Schmitz, J. M. Carlin, E. C. Borden, G. I. Byrne, Beta interferon inhibits Toxoplasma gondii growth in human monocyte-derived macrophages. *Infect. Immun.* **57**, 3254–3256 (1989).
21. S. K. Matta, N. Rinkenberger, I. R. Dunay, L. D. Sibley, Toxoplasma gondii infection and its implications within the central nervous system. *Nat. Rev. Microbiol.* **19**, 467–480 (2021).
22. E. R. Pfefferkorn, Interferon-gamma blocks the growth of *Toxoplasma gondii* in human fibroblasts by inducing the host to degrade tryptophan. *Proc. Natl. Acad. Sci. U.S.A.* **81**, 908–912 (1984).
23. W. Daubener *et al.*, Restriction of Toxoplasma gondii growth in human brain microvascular endothelial cells by activation of indoleamine 2,3-dioxygenase. *Infect. Immun.* **69**, 6527–6531 (2001).
24. E. M. Selleck *et al.*, A noncanonical autophagy pathway restricts *Toxoplasma gondii* growth in a strain-specific manner in IFN-gamma–activated human cells. *mBio* **6**, e01157–15 (2015).
25. J. Bhushan *et al.*, ISG15 connects autophagy and IFN-gamma-dependent control of Toxoplasma gondii infection in human cells. *mBio* **11**, e00852-20 (2020).
26. B. Clough *et al.*, K63-linked ubiquitination targets Toxoplasma gondii for endo-lysosomal destruction in IFNgamma-stimulated human cells. *PLoS Pathog.* **12**, e1006027 (2016).
27. D. Hernandez, S. Walsh, L. Saavedra Sanchez, M. S. Dickinson, J. Coers, Interferon-inducible E3 ligase RNF213 facilitates host-protective linear and K63-linked ubiquitylation of Toxoplasma gondii parasitophorous vacuoles. *mBio* **13**, e0188822 (2022), 10.1128/mbio.01888-22.
28. A. C. Johnston *et al.*, Human GBP1 does not localize to pathogen vacuoles but restricts Toxoplasma gondii. *Cell Microbiol.* **18**, 1056–1064 (2016).
29. D. Fisch *et al.*, Human GBP1 is a microbe-specific gatekeeper of macrophage apoptosis and pyroptosis. *EMBO J.* **38**, e100926 (2019).
30. D. Fisch, B. Clough, R. Khan, L. Healy, E. M. Frickel, Toxoplasma-proximal and distal control by GBPs in human macrophages. *Pathog. Dis.* **79**, ftab058 (2022).
31. N. Rinkenberger *et al.*, Overexpression screen of interferon-stimulated genes identifies RARRES3 as a restrictor of Toxoplasma gondii infection. *Elife* **10**, e73137 (2021).
32. J. G. Doench *et al.*, Optimized sgRNA design to maximize activity and minimize off-target effects of CRISPR-Cas9. *Nat. Biotechnol.* **34**, 184–191 (2016).
33. W. Li *et al.*, Merlin/NF2 suppresses tumorigenesis by inhibiting the E3 ubiquitin ligase CRL4(DCAF1) in the nucleus. *Cell* **140**, 477–490 (2010).
34. J. G. Doench, Am I ready for CRISPR? A user's guide to genetic screens. *Nat. Rev. Genet.* **19**, 67–80 (2018).
35. H. Feng, Y. B. Zhang, J. F. Gui, S. M. Lemon, D. Yamane, Interferon regulatory factor 1 (IRF1) and anti-pathogen innate immune responses. *PLoS Pathog.* **17**, e1009220 (2021).
36. E. G. Otten *et al.*, Ubiquitylation of lipopolysaccharide by RNF213 during bacterial infection. *Nature* **594**, 111–116 (2021).
37. M. Fujimuro, H. Sawada, H. Yokosawa, Production and characterization of monoclonal antibodies specific to multi-ubiquitin chains of polyubiquitinated proteins. *FEBS Lett.* **349**, 173–180 (1994).
38. D. Houzelstein *et al.*, The ring finger protein 213 gene (Rnf213) contributes to Rift Valley fever resistance in mice. *Mamm. Genome.* **32**, 30–37 (2021).
39. D. Fisch *et al.*, Human GBP1 differentially targets Salmonella and Toxoplasma to license recognition of microbial ligands and caspase-mediated death. *Cell Rep.* **32**, 108008 (2020).
40. S. M. White *et al.*, YAP/TAZ inhibition induces metabolic and signaling rewiring resulting in targetable vulnerabilities in NF2-deficient tumor cells. *Dev. Cell* **49**, 425–443.e9 (2019).
41. T. Taniguchi, K. Ogasawara, A. Takaoka, N. Tanaka, IRF family of transcription factors as regulators of host defense. *Annu. Rev. Immunol.* **19**, 623–655 (2001).
42. M. F. James *et al.*, NF2/merlin is a novel negative regulator of mTOR complex 1, and activation of mTORC1 is associated with meningioma and schwannoma growth. *Mol. Cell Biol.* **29**, 4250–4261 (2009).
43. S. Butterworth *et al.*, Toxoplasma gondii virulence factor ROP1 reduces parasite susceptibility to murine and human innate immune restriction. *PLoS Pathog.* **18**, e1011021 (2022).
44. F. Thery *et al.*, Ring finger protein 213 assembles into a sensor for ISGylated proteins with antimicrobial activity. *Nat. Commun.* **12**, 5772 (2021).
45. S. C. Walsh *et al.*, The bacterial effector GarD shields Chlamydia trachomatis inclusions from RNF213-mediated ubiquitylation and destruction. *Cell Host Microbe* **30**, 1671–1684.e9 (2022), 10.1016/j.chom.2022.08.008.
46. D. Mukhopadhyay, D. Arranz-Solis, J. P. J. Saeij, Toxoplasma GRA15 and GRA24 are important activators of the host innate immune response in the absence of TLR11. *PLoS Pathog.* **16**, e1008586 (2020).
47. L. O. Sangare *et al.*, Toxoplasma GRA15 activates the NF-kappaB pathway through interactions with TNF receptor-associated factors. *mBio* **10**, e00808-19 (2019).
48. J. Ahel *et al.*, Moyamoya disease factor RNF213 is a giant E3 ligase with a dynein-like core and a distinct ubiquitin-transfer mechanism. *Elife* **9**, e56185 (2020).
49. J. B. Radke *et al.*, Bicyclic azetidines target acute and chronic stages of Toxoplasma gondii by inhibiting parasite phenylalanyl t-RNA synthetase. *Nat. Commun.* **13**, 459 (2022).
50. B. Wang *et al.*, Integrative analysis of pooled CRISPR genetic screens using MAGeCKFlute. *Nat. Protoc.* **14**, 756–780 (2019).
51. S. K. Matta, L. David Sibley, IFN-γ induced transcriptional profile of A549 cells in absence of key transcriptional regulators IRF1 and NF2. URL. https://www.ncbi.nlm.nih.gov/geo/query/acc.cgi?acc=GSE215771. Deposited 14 October 2022.